Eur. Phys. J. D **9**, 69–75 (1999)

THE EUROPEAN PHYSICAL JOURNAL D

EDP Sciences

The remarkable properties of carbon nanotubes as nanoclusters

M.S. Dresselhaus[1,2], G. Dresselhaus[3], and M. Pimenta[1,4]

[1] Department of Physics, Massachusetts Institute of Technology, Cambridge, MA 02139, USA
[2] Department of Electrical Engineering and Computer Science, Massachusetts Institute of Technology, Cambridge, MA 02139, USA
[3] Francis Bitter Magnet Laboratory, Massachusetts Institute of Technology, Cambridge, MA 02139, USA
[4] Departamento de Fisica, Universidade Federal de Minas Gerais, Belo Horizonte, 30123-970, Brazil

Received: 3 September 1998 / Received in final form: 20 October 1998

Abstract. A brief overview will be given of the unique structure and properties of carbon nanotubes (diameters ~ 1.3 nm). The remarkable electronic properties of carbon nanotubes relate to predictions and observations that these structures can be either semiconducting or metallic, depending on their geometry. Resonant Raman scattering along with scanning tunneling microscopy/spectroscopy have provided a powerful characterization tool for probing the one-dimensional (1D) density of electronic states of the carbon nanotubes, while also providing important information on the structure and lattice vibrational modes in these unique 1D nanostructures.

PACS. 78.30.Jw Organic solids, polymers

1 Introduction

Carbon nanotubes are highly ordered clusters which display remarkable electronic properties, that arise from the special properties of their one-dimensional (1D) density of states. Early calculations [1–3] in 1992 indicated that carbon nanotubes could be either semiconducting or metallic, depending on their diameter and the orientation of the carbon hexagons of the honeycomb structure of the cylindrical tubes with respect to the nanotube axis (see Fig. 1) [1–3]. These remarkable electronic properties are now beginning to be confirmed experimentally, both by scanning tunneling microscopy and by resonant Raman scattering studies. In this paper we review the present status of this field of nano-cluster science.

The single wall carbon nanotubes (SWNT) can be considered as a very large molecule or a molecular cluster. Because of the large aspect ratio (length to diameter) of carbon nanotubes, the energy levels associated with the degree of freedom along the nanotube axis direction are very closely spaced, which for most applications can be considered as a quasi-continuum, while the number of allowed k vectors in the circumferential direction is small. Therefore the quasi-continuum of states along the nanotube axis can be described in terms of a 1D density of states. Because the lengths of the nanotubes are in the micrometer range, the discreteness of the levels associated with the nanotube direction (quantum dot limit) has been demonstrated in elegant transport measurements on an individual SWNT [5].

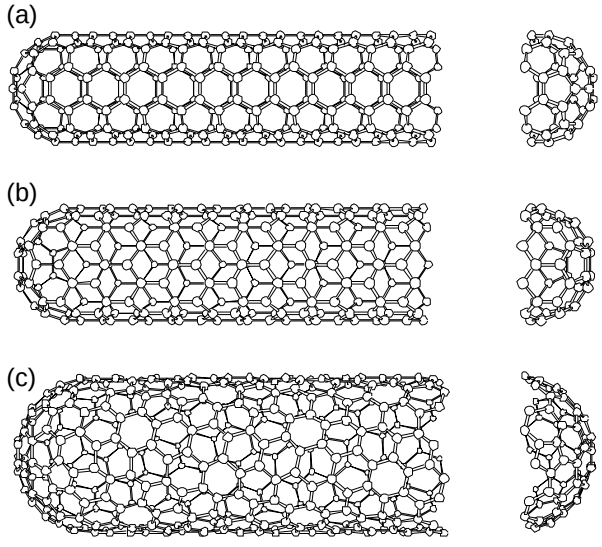

Fig. 1. Schematic models for single-wall carbon nanotubes. (a) an "armchair" (n, n) nanotube, (b) a "zigzag" $(n, 0)$ nanotube, and (c) a "chiral" (n, m) nanotube $(n \neq m)$ [4].

2 The 1D density of states

It is convenient to discuss the remarkable electronic properties of the single wall nanotubes in terms of their electronic density of states. Assuming these states form a quasi-continuum, theoretical calculations provide the general form for the 1D density of states [6, 7]. This gen-

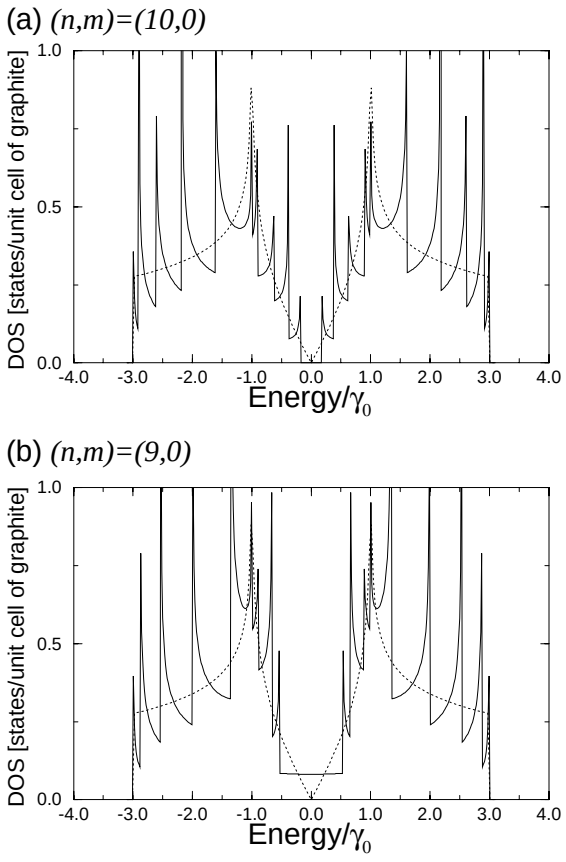

Fig. 2. Electronic 1D density of states (DOS) per unit cell of a 2D graphene sheet for two $(n, 0)$ zigzag nanotubes: (a) the $(10, 0)$ nanotube which has semiconducting behavior, (b) the $(9, 0)$ nanotube which has metallic behavior. Also shown in the figure is the density of states for the 2D graphene sheet (dotted line) [9]. $\mathcal{E}_{11}$ is the smallest energy difference between two singularities in the density of states that spans the Fermi level at $E_{\rm F} = 0$.

eral framework is shown in Fig. 2 for a semiconducting [Fig. 2(a)] and a metallic [Fig. 2(b)] nanotube. Although the results are shown here explicitly for zigzag nanotubes [see Fig. 1(b)], the general framework is common to all semiconducting nanotubes [Fig. 2(a)] and all metallic nanotubes [Fig. 2(b)].

The 1D density of electronic states in Fig. 2 show sharp features associated with the $(E - E_{0i})^{-1/2}$ singularities which occur at E_{0i}, the energy of each subband edge i. The results in Fig. 2 further show that the metallic nanotubes have a small, but non-vanishing 1D density of states at the Fermi level $E_{\rm F}$ (which is at $E = 0$ in Fig. 2). This non-vanishing density of states is independent of energy until the energies of the first subband edges of the valence and conduction bands are reached. We denote the energy separation between the valence subband edge i and conduction subband edge j by $\mathcal{E}_{ij}$, so that $\mathcal{E}_{11}$ denotes the smallest possible energy separation that spans the Fermi level. In contrast, for a 2D graphene sheet (dotted curve) corresponding to a nanotube of infinite diameter, the 2D density of states is zero at the Fermi level (where $E = 0$ in Fig. 2), and varies linearly with energy, as we move away from the Fermi level.

In contrast to the behavior of the 1D metallic nanotubes, the density of states for the semiconducting 1D nanotubes is zero throughout the bandgap, as shown in Fig. 2(a), and in this case the bandgap energy E_g is equal to the energy difference $\mathcal{E}_{11}$ between the two singularities in the 1D density of states that span the Fermi level. Because of the occurrence of these singularities in the 1D density of states, high optical absorption is expected when the photon energy matches the energy separation between an occupied electron band edge state and one that is empty. This high absorption probability occurs not only at the band gap $\mathcal{E}_{11}$ for the semiconducting nanotubes, but also at higher energies (such as $\mathcal{E}_{22}$). Calculations [8] show that transitions have a much higher probability to occur when $i = j$ in $\mathcal{E}_{ij}$, in comparison to transitions for which $i \neq j$. Transitions $\mathcal{E}_{ij}$ $(i = j)$ between subband edge states can occur for both semiconducting and metallic nanotubes.

Comparing the density of states curves for metallic and semiconducting nanotubes in Fig. 2, we see that the smallest energy separation between subband edge states for the metallic nanotube (9,0) is much larger than that for the semiconducting (10,0) nanotube [10–12]. Here each tube is denoted by a pair of indices (n, m), which, respectively, specify the number of $\mathbf{a}_1$ and $\mathbf{a}_2$ lattice vectors of the 2D honeycomb lattice that are contained in the chiral vector or "roll-up vector", which defines the geometry of each cylindrical nanotube [6, 7]. The actual nanotubes shown in Fig. 1 correspond to (n, m) values of: (a) (5, 5), (b) (9, 0), and (c) (10, 5), respectively. With increasing nanotube diameter, the number of energy subbands increases and the spacing between the singularities in the 1D density of states decreases, as does the value of $\mathcal{E}_{ii}$ for given i, and the magnitude of E_g for semiconducting nanotubes.

The condition that a nanotube is metallic is that $n - m = 3q$ where q is an integer [6], as shown in Fig. 3. Here we see that 2/3 of the possible single wall nanotubes that can be formed are semiconducting, and the remaining 1/3 are metallic. Thus a (10,10) carbon nanotube (diameter $d_t = 1.375$ nm) is metallic, while the (11,9) nanotube of almost the same diameter (diameter $d_t = 1.377$ nm) is semiconducting and is predicted to have very different electronic properties.

The two experiments which have thus far provided the most valuable information about the 1D electronic density of states are scanning tunneling spectroscopy (STS), and resonant Raman scattering experiments, while high resolution transmission electron microscopy (TEM) and scanning tunneling microscopy (STM) studies have been most informative regarding structural information, showing that single-wall carbon nanotubes can indeed be considered as rolled up seamless cylinders of flat graphene sheets of sp^2 bonded carbon atoms organized into a honeycomb structure (see Fig. 1).

The most promising direct technique for carrying out sensitive measurements of the electronic properties of individual nanotubes is high resolution scanning tunneling spectroscopy (STS) because of the ability of the tunneling tip to sensitively probe the electronic density of states of

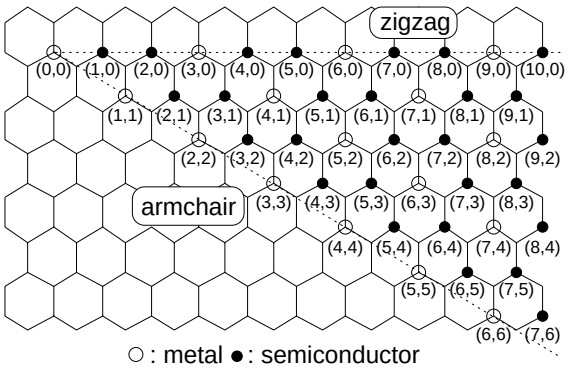

Fig. 3. The carbon nanotubes (n, m) that are metallic and semiconducting, respectively, are denoted by open and solid circles on the map of chiral vectors (n, m). All possible chiral vectors $\mathbf{C}_h = n\mathbf{a}_1 + m\mathbf{a}_2$ are specified by the pairs of integers (n, m) for general carbon nanotubes, including zigzag, armchair, and chiral nanotubes. According to theoretical calculations, the encircled dots denote metallic nanotubes, while the small dots denote semiconducting nanotubes [13].

an individual single-wall nanotube [10, 11, 14] or the outermost cylinder of a multi-wall nanotube [15], due to the exponential dependence of the tunneling current on the distance between the nanotube and the tunneling tip. With this technique, it is further possible to carry out both STS and STM measurements on the same individual nanotube, and therefore to measure the nanotube structure concurrently with the STS electronic spectrum [15].

In early pioneering STM/STS studies, more than nine individual multi-wall nanotubes with diameters d_t ranging from 1.7 to 9.5 nm were examined. Topographic STM measurements were made on the same nanotubes to obtain the maximum height of the nanotube relative to the gold substrate, thus determining the diameter of each individual nanotube [15]. Then switching to the STS mode of operation, current–voltage (I vs V) plots were made on the same region of the same nanotube as had been just characterized for its diameter by the STM mode of operation. These early results provided evidence for both metallic and semiconducting outer walls for their multi-wall nanotubes [15]. The results for all their semiconducting nanotubes showed a linear dependence of their energy gaps on $1/d_t$, consistent with the predicted functional form [6, 7].

Subsequently, more detailed low temperature atomic resolution STM/STS experiments were carried out on single-wall carbon nanotubes [10, 11]. By taking the images under atomic resolution conditions, the characterization of individual single-wall nanotubes could be made, yielding both their diameters and chiral angles [or equivalently their (n, m) indices] [10]. Measurements of $\mathrm{d}I/\mathrm{d}V$ in the STS mode, yielded the 1D density of states (which is proportional to $\mathrm{d}I/\mathrm{d}V$) for both metallic and semiconducting nanotubes. The results of the various STM/STS studies [10, 11, 15] are consistent with many of the theoretical predictions: (1) that about 2/3 of the nanotubes are semiconducting, and 1/3 are metallic; (2) that the density of states exhibits singularities that are characteristic of the expectations for 1D systems; (3) that the band gap E_g for the semiconducting nanotubes is proportional to $1/d_t$ with $E_g = 2\gamma_0 a_{\text{C-C}}/d_t$, thus yielding a value for the nearest neighbor overlap integral γ_0 (or transfer integral) of 2.7 eV from the STS data [10], in good agreement with theoretical predictions, where $a_{\text{C-C}}$ is the nearest neighbor carbon-carbon distance; and (4) that the density of states near the Fermi level is zero for semiconducting nanotubes, and non-zero for metallic nanotubes [10, 11]. These density of states curves are also important for explaining the quantum effects observed in the resonant Raman experiments on carbon nanotubes discussed below.

3 Resonant Raman spectroscopy

Resonant Raman spectroscopy has become an important technique for providing information on the electronic density of states, insofar as the resonant Raman process is sensitive to the electronic structure through the electron-phonon interaction. The singularities in the 1D density of states (Fig. 2) give rise to a large Raman signal, for both semiconducting and metallic nanotubes, when the laser excitation energy for Raman scattering corresponds to an energy $\mathcal{E}_{ii}$ for which there is strong optical absorption due to the large value of the joint density of states (see Fig. 2). Since a given sample of single wall nanotubes has a distribution of nanotube diameters ($\pm 10\%$) and therefore also of (n, m) values, a given laser excitation energy $\mathcal{E}_{\text{L}}$ will result in a large cross section only for those single wall nanotubes for which $\mathcal{E}_{\text{L}} = \mathcal{E}_{ii}$. Thus the resonant Raman process is selective of only those carbon nanotubes that have (n, m) values which give rise to energy differences $\mathcal{E}_{ii}$ that fall within the narrow linewidth of the laser energy $\mathcal{E}_{\text{L}}$.

We now discuss the various features of the resonant Raman spectra and the information they provide about the carbon nanotube structure and properties. A typical Raman spectrum for a single wall carbon nanotube sample is shown in Fig. 4. This spectrum is unique among carbon based materials and has several interesting features. At low frequency shifts, we see a strong feature at 186 cm^{-1}, which is identified with the radial breathing mode, where all carbon atoms in the nanotube vibrate in phase in a radial direction relative to the nanotube axis. The strong doublet feature with resolved peaks at 1567 and 1593 cm^{-1} corresponds to the superposition of several Raman-active C-C tangential modes, related to the E_{2g_2} Raman-active mode in a graphene layer [17], as shown in the inset to Fig. 4. The highly dispersive mode near 1347 cm^{-1} in the spectrum taken at 514.5 nm (Fig. 5) is identified with the disordered D-band process which is observed in all disordered carbons. The other weak features in the spectrum have been attributed to finite size effects related to the development of an electric dipole moment for a nanotube that is small in length compared to λ_L, the wavelength of the excitation laser [18].

One reason why the Raman spectra of all carbon nanotubes have these common spectral features arises because

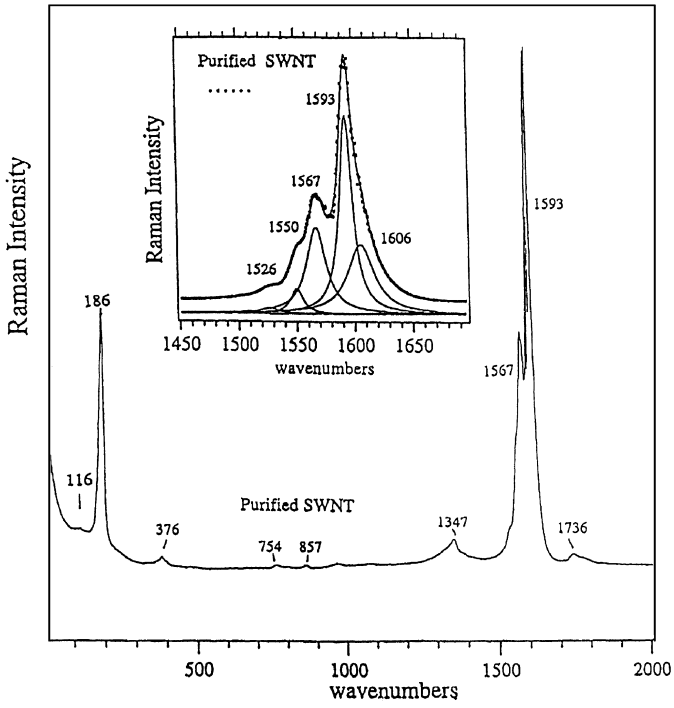

Fig. 4. Experimental Raman spectrum [16] taken with 514.5 nm laser excitation from a sample consisting primarily of single-wall nanotubes with diameters d_t in the range 1.2–1.4 nm, prepared by the laser vaporization technique.

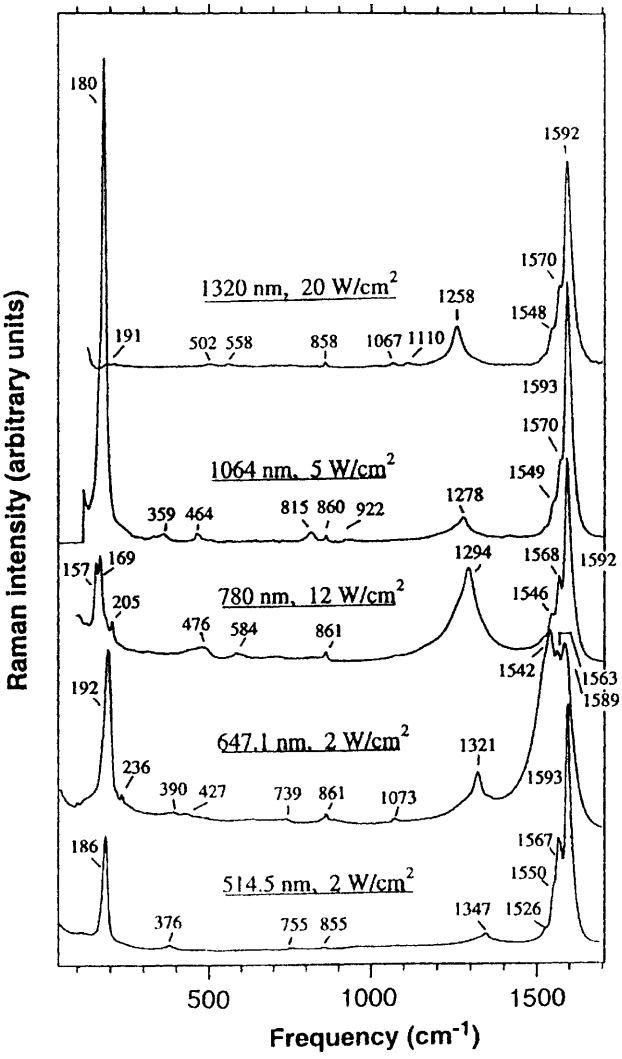

Fig. 5. Experimental room temperature Raman spectra for purified single-wall carbon nanotubes excited at five different laser excitation wavelengths. The laser wavelength and power density for each spectrum are indicated, as are the vibrational frequencies (in cm^{-1}) [16]. The equivalent photon energies for the laser excitation are: 1320 nm $\rightarrow$ 0.94 eV; 1064 nm $\rightarrow$ 1.17 eV; 780 nm $\rightarrow$ 1.58 eV; 647.1 nm $\rightarrow$ 1.92 eV; 514.5 nm $\rightarrow$ 2.41 eV.

of another unique property of single wall carbon nanotubes, namely that the number of Raman-active modes is the same for any nanotube with a given type of symmetry. For example, all chiral nanotubes have 15 Raman-active mode frequencies, with symmetries $(4A+5E_1+6E_2)$, independent of their diameter or chiral angle. Thus, although the number of normal modes increases as the diameter of the nanotube increases, the number of Raman-active and infrared-active modes remains the same for nanotubes with the same symmetry (see Fig. 1). This remarkable property about carbon nanotubes allows us to compare the Raman spectra of different nanotubes easily. Specifically, this property allows us to study the dependence of a particular vibrational mode on nanotube diameter, thereby providing important information about the physical properties of the single wall carbon nanotubes, as discussed below.

Theoretical calculations [8, 19] suggest that many of the mode frequencies are highly sensitive to the nanotube diameter, while others are not. Figure 6 shows the calculated dependence of the frequency of the Raman-active modes of armchair nanotubes on the nanotube diameter, expressed in terms of their (n, n) indices [20]. These calculations show that the low frequency A_{1g} radial breathing mode is strongly dependent on nanotube diameter, while the high frequency modes near $1580\,cm^{-1}$ are not. Similar diagrams can be constructed for the Raman-active modes for zigzag and chiral nanotubes [6, 20]. Direct calculations [19] show that the frequencies of the radial breathing mode depends inversely as the nanotube diameter, and is independent of the chiral angle because all the carbon atoms in the nanotube vibrate in phase in a radial direction. Direct experimental evidence that the radial breathing mode frequency is dependent on the nanotube diameter comes from studies of the resonant Raman spectra by measuring these spectra at a number of laser excitation energies $\mathcal{E}_L$, as shown in Fig. 5. As discussed above, resonant enhancement in the Raman scattering intensity from carbon nanotubes occurs when the laser excitation frequency corresponds to a transition between the sharp features in the one-dimensional electronic density of states, as illustrated in Fig. 7 for the armchair nanotubes (8,8), (9,9), (10,10), and (11,11) [16].

Since the energies of these sharp features in the density of states are strongly dependent on the nanotube diam-

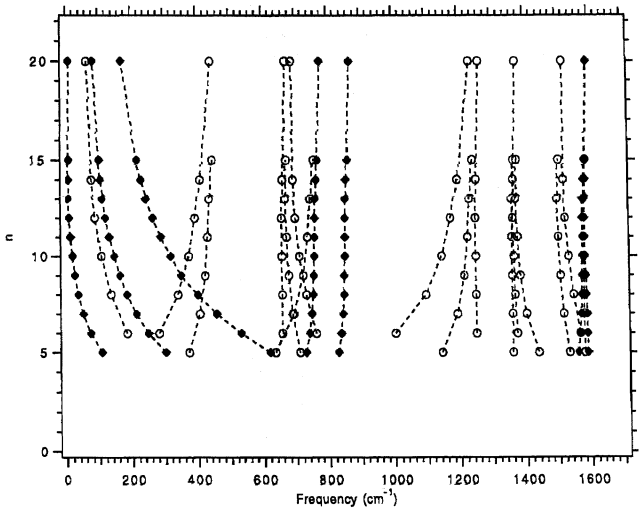

Fig. 6. The armchair index n vs mode frequency for the Raman-active modes of single-wall armchair (n, n) carbon nanotubes [16]. The nanotube diameter d_t can be found from the (n, m) indices from the relation $d_t = \sqrt{3}a_{\text{C-C}}(m^2 + n^2 + nm)^{1/2}/\pi$.

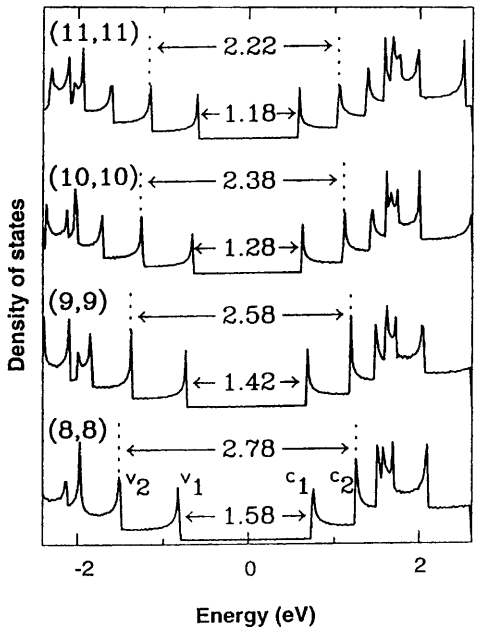

Fig. 7. Electronic 1D density of states (DOS) calculated in a tight binding model for (8,8), (9,9), (10,10), and (11,11) armchair nanotubes assuming $\gamma_0 = 2.3$ eV. Wavevector conserving optical transitions can occur between singularities in the 1D density of states, such as $v_1 \rightarrow c_1$ and $v_2 \rightarrow c_2$, etc. These optical transitions are responsible for the resonant Raman effect shown in Figs. 5 and 8 [16, 24].

eter, a change in the laser frequency brings into resonance a carbon nanotube with a different diameter. For example, Fig. 7 suggests that the (10,10) armchair nanotube would be resonant at a laser frequency of 1.28 eV, while the (9,9) nanotube would be resonant at 1.42 eV (assuming the low γ_0 value used in this figure). However, armchair nanotubes with different diameters have different vibrational frequencies for the A_{1g} radial breathing mode (see Fig. 6). By comparing the various Raman spectra in Fig. 5, we see large differences in the vibrational frequencies and intensities of the strong A_{1g} radial breathing mode, consistent with a resonant Raman process involving nanotubes of different diameters. Detailed analysis of experimental studies of the radial breathing mode have been carried out in terms of these models by several research groups, yielding results consistent with these predictions. For this reason, measurements of the radial breathing mode frequencies have also been used to estimate the diameter distribution of the carbon nanotubes for actual samples of single wall carbon nanotubes [21–23].

The dependence of the high frequency C-C tangential mode on laser excitation energy $\mathcal{E}_{\text{L}}$ is very different from that for the radial breathing mode described above. The very weak dispersion of the Raman-active phonon bands near 1580 cm^{-1} is reflected in the great similarity of the Raman spectra of Fig. 8 for spectra obtained [24] in the high frequency range (1400–1700 cm^{-1}) with different laser lines from $0.94 \leq \mathcal{E}_{\text{L}} \leq 3.05$ eV. From Fig. 8 we see that the spectra obtained for $\mathcal{E}_{\text{L}}$ in the ranges 0.94–1.59 eV and 2.41–3.05 eV are quite similar. Analysis of such spectra (e.g., the inset to Fig. 4) shows that the resonant band contains a number of Lorentzian components, which arise both from the variety of modes that are resonant in the phonon frequency range 1500–1630 cm^{-1} (see Fig. 6) and from the distribution of tube diameters in the sample. The reason why the spectra appear so similar over this wide range of $\mathcal{E}_{\text{L}}$ is the very small dispersion of the Raman-active modes in the 1500–1630 cm^{-1} range [6–8]. For $\mathcal{E}_{\text{L}}$ in the ranges of 0.94–1.59 eV and 2.41–3.05 eV, the resonant Raman process for single wall carbon nanotubes in the diameter range between 1.2–1.4 nm involves mostly $\mathcal{E}_{22}$ and $\mathcal{E}_{33}$ transitions for predominantly semiconducting nanotubes. However, for the range of $\mathcal{E}_{\text{L}}$ between 1.7–2.2 eV, where the resonant Raman process includes also metallic carbon nanotubes, the spectrum looks completely different [16, 24], as is seen for example, in Fig. 8, where the spectrum obtained with $\mathcal{E}_{\text{L}} = 1.92$ eV is shown in more detail than in Fig. 5 [16].

It is found that the fitting to the spectrum for $\mathcal{E}_{\text{L}} = 1.92$ eV (and for many other spectra taken in the 1.7–2.2 eV range) can be done by superimposing four additional Lorentzian lines to the features found in the Raman band taken at 2.41 eV (outside the 1.7–2.2 eV range). The frequencies of these four, broad additional peaks are: 1515, 1540, 1558 and 1581 cm^{-1}, and these peaks are identified with metallic nanotubes and dominate the spectrum taken at 1.92 eV. The presence of Lorentzian components common to the spectra in the 2.41–3.05 eV range, may be due to semiconducting nanotubes resonant in this range, or may also be a characteristic feature of metallic nanotubes. The special features in the Raman spectra for the metallic nanotubes are likely due to the interaction of the conduction electrons with the lattice vibrations.

Calculations of the 1D density of states for carbon nanotubes with diameters in the 1.2–1.4 nm range and $\gamma_0 = 3$ eV, which is a good approximation for graphite [25],

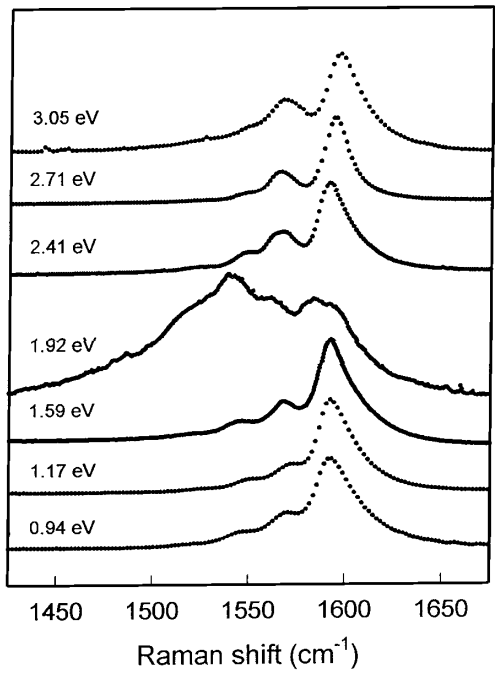

Fig. 8. Raman spectra of the tangential, high frequency C-C stretching modes of single-wall carbon nanotubes obtained with different excitation energies $\mathcal{E}_{\mathrm{L}}$ [24].

give excellent agreement with a detailed analysis of the dependence of the four special features of the resonant Raman spectra on $\mathcal{E}_{\mathrm{L}}$ in the 1.7–2.3 eV range [26]. This work thus identifies the $\mathcal{E}_{11}$ transition for metallic nanotubes as the resonant process associated with these four special spectral features. The value of $\gamma_0 = 2.95$ eV which emerges from this fitting procedure is in good agreement with the determination of γ_0 from scanning tunneling spectroscopy measurements on single wall carbon nanotubes. The small downshift of γ_0 relative to crystalline graphite ($\gamma_0 = 3.18$ eV) may be related to small differences in lattice constant and nanotube curvature.

4 Concluding remarks

The remarkable electronic properties of single wall carbon nanotubes, allowing them to be either semiconducting or metallic depending on purely geometrical factors, are shown to be related to the properties of the individual 1D cluster. Since the carbon nanotube dispersion relations (both electron and phonon) are well explained by Brillouin zone folding of the relations for a graphene sheet, the perturbations relating to the nanotube curvature and the interactions between adjacent nanotubes in a crystalline array of nanotubes are small. Resonant Raman scattering and scanning tunneling spectroscopy provide direct evidence for the 1D density of states, first predicted theoretically, and clearly distinguish metallic from semiconducting nanotubes. Finer details associated with nanotube chirality, tube-tube interaction, and the exact symmetry of the nanotubes is not sensitively probed by Raman experiments carried out thus far. Further work may in the future show effects related to the singularities in the 1D phonon density of states.

We gratefully acknowledge the stimulating discussions with Professors Morinobu Endo, Riichiro Saito, Jean-Christophe Charlier and Peter Eklund. We are also in debt to many other colleagues for assistance and helpful discussions. The research at MIT is funded by NSF grant DMR-98-04734 and M.A.P. is thankful to the Brazilian agency CAPES for financial support during his visit to MIT.

References

1. R. Saito, G. Dresselhaus, M.S. Dresselhaus: Chem. Phys. Lett. **195**, 537 (1992)
2. J.W. Mintmire, B.I. Dunlap, C.T. White: Phys. Rev. Lett. **68**, 631 (1992)
3. T. Hamada, M. Furuyama, T. Tomioka, M. Endo: J. Mater. Res. **7**, 1178 (1992); ibid., 2612
4. M.S. Dresselhaus, G. Dresselhaus, R. Saito: Carbon **33**, 883 (1995)
5. S.J. Tans, M.H. Devoret, H. Dai, A. Thess, R.E. Smalley, L.J. Geerligs, C. Dekker: Nature (London) **386**, 474 (1997)
6. M.S. Dresselhaus, G. Dresselhaus, P.C. Eklund: *Science of Fullerenes and Carbon Nanotubes* (Academic Press, New York, NY 1996)
7. R. Saito, G. Dresselhaus, M.S. Dresselhaus: *Physical Properties of Carbon Nanotubes* (Imperial College Press, London, 1998)
8. E. Richter, K.R. Subbaswamy: Phys. Rev. Lett. **79**, 2738 (1997)
9. R. Saito, G. Dresselhaus, M.S. Dresselhaus: J. Appl. Phys. **73**, 494 (1993)
10. J.W.G. Wildöer, L.C. Venema, A.G. Rinzler, R.E. Smalley, C. Dekker: Nature (London) **391**, 59 (1998)
11. T.W. Odom, J.L. Hung, P. Kim, C.M. Limber: Nature (London) **391**, 62 (1998)
12. M.S. Dresselhaus: Nature (London) **391**, 19 (1998)
13. M.S. Dresselhaus, G. Dresselhaus, R. Saito: Phys. Rev. B **45**, 6234 (1992)
14. S. Wang, D. Thou: Chem. Phys. Lett. **225**, 165 (1994)
15. C.H. Olk, J.P. Heremans: J. Mater. Res. **9**, 259 (1994)
16. A.M. Rao, E. Richter, S. Bandow, B. Chase, P.C. Eklund, K.W. Williams, M. Menon, K.R. Subbaswamy, A. Thess, R.E. Smalley, G. Dresselhaus, M.S. Dresselhaus: Science **275**, 187 (1997)
17. M.S. Dresselhaus, G. Dresselhaus, P.C. Eklund: J. Raman Spectrosc. **27**, 351 (1995)
18. R. Saito, T. Takeya, T. Kimura, G. Dresselhaus, M.S. Dresselhaus: Phys. Rev. B **59**, 2388 (1999)
19. R. Saito, T. Takeya, T. Kimura, G. Dresselhaus, M.S. Dresselhaus: Phys. Rev. B **57**, 4145 (1998)
20. P.C. Eklund, J.M. Holden, R.A. Jishi: Carbon **33**, 959 (1995)
21. A. Kasuya, Y. Sasaki, Y. Saito, K. Tohji, Y. Nishina: Phys. Rev. Lett. **78**, 4434 (1997)

22. A. Kasuya, M. Sugano, Y. Sasaki, T. Maeda, Y. Saito, K. Tohji, H. Takahashi, Y. Sasaki, M. Fukushima, Y. Nishina, C. Horie: Phys. Rev. B **57**, 4999 (1998)
23. H. Kuzmany: In *Optical and Electronic Properties of Fullerenes and Fullerene-Based Materials*, ed. by J. Shinar, Z.V. Vardeny, Z.H. Kafafi, page xx (Marcel Dekker, New York 1999), Chapt. 5
24. M.A. Pimenta, A. Marucci, S.D.M. Brown, M.J. Matthews, A.M. Rao, P.C. Eklund, R.E. Smalley, G. Dresselhaus, M.S. Dresselhaus: J. Mater. Res. **13**, 2396 (1998)
25. M.S. Dresselhaus, G. Dresselhaus: Adv. Phys. **30**, 139 (1981)
26. M.A. Pimenta, A. Marucci, S. Empedocles, M. Bawendi, E.B. Hanlon, A.M. Rao, P.C. Eklund, R.E. Smalley, G. Dresselhaus, M.S. Dresselhaus: Phys. Rev. B **58**, R16 012 (1998)